Polarization observables in dp backward elastic scattering at high and intermediate energies

M. Tanifuji[a,], S. Ishikawa[a,1] and Y. Iseri[b]

[a] *Department of Physics, Hosei University, Fujimi 2-17-1, Chiyoda, Tokyo 102, Japan*

[b] *Department of Physics, Chiba-Keizai College, Todoroki-cho 4-3-30, Inage-ku, Chiba 263, Japan*

Abstract

The tensor analyzing power T_{20} and the polarization transfer coefficients $\kappa_0(=\frac{3}{2}K_y^y)$ and K_{xz}^y are investigated for dp backward elastic scattering by the invariant-amplitude method. Discrepancies between the conventional calculations and the experimental data on T_{20} and κ_0 at high and intermediate energies are mostly dissolved by including imaginary parts in the amplitudes. The quantity K_{xz}^y is shown to be useful in criticizing nuclear force assumptions.

PACS: 21.30.-x, 21.45.+v, 24.70.+s, 25.10.+s

Keywords: Polarization observable; dp backward elastic scattering; One nucleon exchange model; Invariant amplitude

[1]E-mail: ishikawa@fujimi.hosei.ac.jp

Polarization phenomena in few-body systems are important sources of information on nuclear forces and related dynamics. In particular, the tensor analyzing power T_{20} and the polarization transfer coefficient from deuterons to protons $\kappa_0 (= \frac{3}{2} K_y^y)$ in backward elastic scattering of the deuteron by the proton at high and intermediate energies have attracted attention because of serious discrepancies between the theoretical prediction [1, 2] and the recent experimental data [3]. For example, the quantities calculated by the PWIA with the one nucleon exchange (ONE) model [1, 2], which describes the dominant mechanism at backward angles, satisfy the equation of a circle in the $\kappa_0 - T_{20}$ plane [2], while the measured ones deviate remarkably from the circle along a spiral-like curve. The observables for the inclusive deuteron breakup also suffer from similar difficulties [3]. Several theoretical investigations [4, 5], which include QCD effects for example, have been attempted but the puzzle still remains to be unsolved.

In the present note, we will derive formulae of the polarization observables, T_{20}, κ_0 and K_{xz}^y, for the dp backward elastic scattering by the invariant-amplitude method [6] in the non-relativistic framework, assuming the ONE mechanism. Using the formulae, where the observables are described in terms of the invariant amplitudes, we investigate general effects of imaginary parts of the amplitudes, evaluating the magnitudes of the amplitudes by the PWIA. The imaginary parts produce important effects on the observables and most of the discrepancies discussed above can be dissolved by the effects. Recently, model-independent formulae of T_{20} and κ_0 in (d,p) reactions have been derived [7] by the method similar to the present one. However, they are applicable to the present scattering only at low energies because of additional approximations. The present work extends the theory to treat the scattering in a way free from such approximations.

The invariant-amplitude method gives T-matrix ($\mathbf{M}$) elements for a reaction aA→bB,

$$\begin{aligned} \langle \nu_b, \nu_B; \mathbf{k}_f | \mathbf{M} | \nu_a, \nu_A; \mathbf{k}_i \rangle &= \sum_{s_i s_f K} (s_a s_A \nu_a \nu_A | s_i \nu_i)(s_b s_B \nu_b \nu_B | s_f \nu_f)(-)^{s_f - \nu_f} (s_i s_f \nu_i - \nu_f | K \kappa) \\ &\quad \times \sum_{l_i = \bar{K} - K}^{K} [C_{l_i}(\hat{k}_i) \otimes C_{l_f = \bar{K} - l_i}(\hat{k}_f)]^K_\kappa F(s_i, s_f, K, l_i), \end{aligned} \tag{1}$$

where C_{lm} is related to Y_{lm} as usual. The quantity $s(\nu)$ is the spin(z-component), $K(\kappa)$ denotes the rank (z-component) of tensors which classifies the transition amplitudes according to the tensorial character in the spin space, $F(s_i, s_f, K, l_i)$ is the invariant ampli-

tude which is a function of scattering angle θ and the CM energy, and $\bar{K}$ is K for K =even and $K+1$ for K =odd when the parity is unchanged as in the present case.

The non-vanishing matrix elements at $\theta = \pi$ are the following four independent ones which have been derived by the helicity conservation in Ref. [5]. At the present, we will calculate them by the use of Eq. (1). In the coordinate system, y $\parallel \mathbf{k}_i \times \mathbf{k}_f$ and z $\parallel \mathbf{k}_i$,

$$\langle 1, \frac{1}{2}|\mathbf{M}|1, \frac{1}{2}\rangle = \frac{1}{2}(U_2 + T_2), \tag{2}$$

$$\langle 1, -\frac{1}{2}|\mathbf{M}|1, -\frac{1}{2}\rangle = \frac{\sqrt{2}}{3}U_1 + \frac{1}{6}U_2 - \frac{2}{3}T_1 - \frac{1}{6}T_2, \tag{3}$$

$$\langle 1, -\frac{1}{2}|\mathbf{M}|0, \frac{1}{2}\rangle = \langle 0, \frac{1}{2}|\mathbf{M}|1, -\frac{1}{2}\rangle = -\frac{1}{3}U_1 + \frac{1}{3\sqrt{2}}U_2 - \frac{1}{3\sqrt{2}}T_1 - \frac{1}{3\sqrt{2}}T_2, \tag{4}$$

$$\langle 0, \frac{1}{2}|\mathbf{M}|0, \frac{1}{2}\rangle = \frac{1}{3\sqrt{2}}U_1 + \frac{1}{3}U_2 + \frac{2}{3}T_1 - \frac{1}{3}T_2, \tag{5}$$

where $\mathbf{k}_i$ and $\mathbf{k}_f$ in the bracket are discarded to avoid confusions. Here $U_j (j = 1, 2)$ and $T_j (j = 1, 2)$ are the scalar amplitudes and the second-rank tensor ones, respectively, and the scalar ones (tensor ones) describe the scattering by the spin-space scalar (tensor) interactions. The tensor amplitudes include effects of the D-state admixture in the deuteron ground-state wave function. They are given as

$$U_j = F(\frac{2j-1}{2}, \frac{2j-1}{2}, 0, 0), \tag{6}$$

$$T_j = F(\frac{3}{2}, \frac{2j-1}{2}, 2, 0) - \sqrt{\frac{2}{3}}F(\frac{3}{2}, \frac{2j-1}{2}, 2, 1) + F(\frac{3}{2}, \frac{2j-1}{2}, 2, 2). \tag{7}$$

Here, we will assume the ONE mechanism, for which $\langle 1, -\frac{1}{2}|\mathbf{M}|1, -\frac{1}{2}\rangle$ will vanish because the spin-down proton in the incident channel cannot form the spin-up deuteron in the final channel due to the lack of the spin flip of the proton as discussed below. In Eq. (3), the contribution of the central interactions to U_j do not give the spin flip and the contribution of the second order of the tensor interactions is cancelled by the residual terms, $-\frac{2}{3}T_1 - \frac{1}{6}T_2$, in the PWIA limit. To take account of this nature of $\langle 1, -\frac{1}{2}|\mathbf{M}|1, -\frac{1}{2}\rangle$, we will impose the condition, $\frac{\sqrt{2}}{3}U_1 + \frac{1}{6}U_2 - \frac{2}{3}T_1 - \frac{1}{6}T_2 = 0$, on the transition amplitudes. Eliminating U_1 by this condition, physical quantities are described in terms of one scalar amplitude U and two tensor ones T and T' defined by

$$U = \frac{9}{2\sqrt{2}}U_2, \qquad T = -T_1 + 2T_2, \qquad T' = T_1 + \frac{1}{4}T_2. \tag{8}$$

For polarization observables, one can reduce the number of the variables by introducing the relative magnitudes and phases between U, T and T',

$$R = \frac{|T|}{|U|},\ R' = \frac{|T'|}{|U|}, \qquad \Theta = \theta_T - \theta_U,\ \Theta' = \theta_{T'} - \theta_U. \tag{9}$$

Then we get

$$T_{20} = \{2\sqrt{2}R\cos\Theta - R^2 - 32R'^2 + 12RR'\cos(\Theta' - \Theta)\}/N_R, \tag{10}$$

$$\kappa_0 = \{\sqrt{2} - R\cos\Theta - 4R'\cos\Theta' - 3\sqrt{2}RR'\cos(\Theta' - \Theta) - 30\sqrt{2}R'^2\}/N_R \tag{11}$$

with

$$N_R = \sqrt{2} + 2\sqrt{2}R^2 + 34\sqrt{2}R'^2 - 4R'\cos\Theta'. \tag{12}$$

These formulae are exact and independent of details of the reaction dynamics except for the restriction by the ONE mechanism. The quantities R, R', Θ and Θ' can be treated as free parameters and will be determined by experimental data of four independent polarization observables. The parameters thus obtained will be useful for finding or criticizing theoretical models as phase shifts are in the usual scattering [8].

The experimental data available at the present are not sufficient for the determination of the four parameters. In the following, we will calculate R and R' by the PWIA which is fundamentally acceptable at high energies, and treat Θ and Θ' as free parameters in the range $-180^\circ \leq \Theta, \Theta' \leq 180^\circ$, by which imaginary parts are included in the invariant amplitudes. The PWIA amplitudes are described by $u(k)$ and $w(k)$, the Fourier transforms of the S and D components of the deuteron internal wave function. By calculating the LHS of Eqs. (2), (4), (5) by the PWIA,

$$U = \frac{9}{\sqrt{2}}\{u^2(k) + \frac{1}{4}w^2(k)\}t(k), \tag{13}$$

$$T = \frac{9}{\sqrt{2}}u(k)w(k)t(k), \qquad T' = \frac{9}{8}w^2(k)t(k), \tag{14}$$

where $t(k)$ is the proton-neutron scattering amplitude at the momentum k. Denoting $w(k)/u(k)$ by r, we get R and R' in the PWIA limit

$$R = \frac{4|r|}{4 + r^2} \quad \text{and} \quad R' = \frac{r^2}{\sqrt{2}(4 + r^2)}. \tag{15}$$

As is shown for typical inter-nucleon potentials [9, 10, 11, 12] in Fig. 1, r decreases from zero to minus infinity with the increase of k, changes its sign at the zero point of $u(k)$, $k = k_0$, and beyond k_0 decreases from plus infinity. Correspondingly, in the PWIA, $\Theta = 180°$ for $k < k_0$ and $\Theta = 0°$ for $k > k_0$, and Θ' is zero independently of k. In general case, at $r = 0$,

$$T_{20} = 0 \quad \text{and} \quad \kappa_0 = 1, \tag{16}$$

which define the point X in the $\kappa_0 - T_{20}$ plane in Figs. 2(a)-2(d) and in the limit $r \to \infty$

$$T_{20} = -\frac{4\sqrt{2}}{9 - \cos\Theta'} \quad \text{and} \quad \kappa_0 = -\frac{7 + \cos\Theta'}{9 - \cos\Theta'}, \tag{17}$$

which are independent of Θ. In the PWIA limit, $T_{20} = -\frac{1}{\sqrt{2}}$ and $\kappa_0 = -1$, which define the point Y in the $\kappa_0 - T_{20}$ plane. In the following, the polarization observables are calculated for given sets of Θ and Θ' by the use of Eqs. (10)-(12) and (15) by varying r from zero to infinity and the calculation is extended by replacing $|r|$ by $-|r|$ to the region $k \geq k_0$.

In Fig. 2(a), the calculated T_{20} and κ_0 are plotted in the $\kappa_0 - T_{20}$ plane for several Θ, where Θ' is fixed to zero. The calculated quantities are independent on the sign of Θ due to Eqs. (10)-(12). For $\Theta' = 0°$, the present Eqs. (10) and (11) are reduced to Eqs. (16) and (17) in Ref. [7], respectively, when r is replaced again by R after the transformation by Eq. (15). Then, Fig. 2(a) is essentially the same as Fig. 3 in the reference. As was discussed there, the point P defined by a set of κ_0 and T_{20} calculated by the PWIA for an arbitrary k moves clockwise along the circle denoted by $\Theta = 180°$, from X to a certain point through Y with the increase of k. The trajectories of the point P similarly defined for other Θ are deformed toward the inside of the circle according to the decrease of Θ from 180° to 90°, where the point for $k = k_0$ is fixed to Y. We call this deformation of the trajectories the "Θ effect". The experimental data [3] for the small k are mostly located between the two lines for $\Theta = 120°$ and 135°. Then the Θ effect is important to describe such small k data.

Figs. 2(b) and 2(c) show effects of finite Θ' for $\Theta' > 0°$ and for $\Theta' < 0°$, respectively, where Θ is fixed to 135°. In Fig. 2(b), the calculations for Θ' larger than 90° are ignored to avoid the complication of the figure. In both of Figs. 2(b) and 2(c), the point P(k_0) which is defined by κ_0 and T_{20} given by Eq. (17) moves on the X–Y straight line from Y toward

the center of the circle with the increase of the magnitude of Θ', accompanied by the corresponding deformation of the trajectories. We call this the "Θ' effect". To reproduce the data for the large k, the Θ' effect is clearly important. In the cases of $\Theta' = 30°$ and $-105°$, for example, the agreement between the calculation and the experiment is much improved compared with the case of the PWIA. To see the pure Θ' effect, the calculations for several Θ' with $\Theta = 180°$ are performed, the results of which are shown in Fig. 2(d), where the calculated are independent on the sign of Θ'. The Θ' effect is quite remarkable for large magnitudes of Θ'. Most of the data for the large k are located between the trajectories calculated with $\Theta' = 105°$ and $120°$, although they miss the agreements with the small k data . For further investigations, we will classify the trajectories of P in these figures, according to their gross behaviour, into the "egg shape", the "cusp" upon the X–Y line and the "*8* shape". In Fig. 2(b), for example, the trajectory for $\Theta' = 30°$ is the egg shape, those for $\Theta' = 60°$ and $90°$ are the cusp and the *8* shape.

To examine the Θ and Θ' effects in more detail, we will plot T_{20} and κ_0 calculated by Eqs. (10)-(12) and (15) with the Paris potential [9] as the function of k. The shown in Figs. 3(a) and 3(b) are for the typical trajectories in Figs. 2(b)-2(d), i.e. for the sets $(\Theta, \Theta') = (135°, 30°)$, $(135°, -105°)$, $(180°, 105°)$, $(180°, 120°)$ and the pure PWIA. The trajectories for the first two sets are the egg shape and those for the third and the fourth are the cusp and the *8* shape, respectively. In Fig. 3(a), the calculations for the former two sets do not give the structure of T_{20}, which is observed experimentally as a local maximum in the range $k = 0.25 - 0.45$ GeV/c, while those for the latter two produce the structures similar to the experimental one. To produce the structure, even in Figs. 2(b)-2(d) T_{20} is required to have a maximum in the range $\infty > r > 0$. In Figs. 2(b)-2(d), such a maximum of T_{20} is seen in the third quadrant of the κ_0–T_{20} plane for the trajectories of the cusp type and the *8* shape type, though unclear because of the broad shape, while the maximum is not seen for those of the egg shape. The experimental data behave like a cusp upon the X–Y line although modified by the two factors, the fluctuation of κ_0 with k in the large k region and the small bump of T_{20} around $k = 0.44$ GeV/c. In Fig. 2(d), such features of the data are demonstrated by connecting the data points by straight lines. In Fig. 3(a), the calculations by the sets $(135°, 30°)$ and $(135°, -105°)$ describe the T_{20} data very well except the structure. In Fig. 3(b), the calculated κ_0 is compared with the

experimental data, where the present calculations except the one for the set (135°, 30°) give agreements with the data better than those in the PWIA, for the large k. Similar numerical calculations are performed for the RSC [10], Nijmegen [11] and Bonn B [12] potentials. As is speculated from their features seen in Fig. 1, the distributions of T_{20} and κ_0 versus k obtained by the Bonn B potential are considerably stretched toward the larger k, while those calculated by other potentials are rather similar to those by the Paris potential.

In the present investigation, we assume Θ and Θ' to be independent of k for the convenience of examining the general effect of the imaginary part of the amplitudes, although there is no justification for such assumptions. To reproduce the experimental data more quantitatively, one will vary Θ and Θ' with k. For example, vary Θ from 135° to 180° with the increase of k and choose Θ' between $-105°$ and $-120°$. In such cases, experimental data of other observables will be necessary to solve possible ambiguities of the parameters. A candidate of such observables is the deuteron-proton polarization transfer coefficient K^y_{xz},

$$K^y_{xz} = 3\{-R\sin\Theta + 5\sqrt{2}RR'\sin(\Theta - \Theta')\}/N_R. \tag{18}$$

The quantity vanishes in the PWIA limit and is sensitive to Θ and Θ' in general case. For example, its sign is changed by the change of the sign of Θ' when $\Theta = 180°$. Fig. 3(c) shows K^y_{xz} calculated for the (Θ, Θ') sets same as those in Figs. 3(a) and 3(b). The quantity calculated for the set $(135°, 30°)$ and that for the set $(135°, -105°)$ behave quite differently from each other with the opposite sign except those at the small k, contrary to their similarity in T_{20}. Also K^y_{xz} will be useful in criticizing the nuclear force assumptions, because it vanishes at $k = k_0$ and k_0 depends on the force assumption, for example $k_0 = 0.39$ and 0.45 GeV/c for the RSC potential and the Bonn B one, respectively.

From the features of the Θ and Θ' effects, one can speculate about the dynamical origin of the effects. Since the Θ effect is important in the small k region, i.e. at low incident energies, it will originate from non-mesonic phenomena like virtual breakup of the deuteron, the effect of which becomes less important at high energies in the usual deuteron scattering [13]. At energies higher than the pion threshold, mesonic effects, which include excitations of Δ and other baryon resonances, will become important. These will be responsible for the Θ' effect. Earlier mesonic contributions have been investigated in Refs.

[14, 15], where the calculations produce some structures of T_{20} which correspond to the one discussed above but the calculated T_{20} at the minimum, which appears around $k \simeq 0.3$ GeV/c, is too much negative compared with the new data [3], which are considerably less negative than the old ones [16] in that region of k. The latter feature of the calculations may be related to the insufficient treatment of the Θ effect. Finally, the application to the inclusive deuteron breakup and the examination of relativistic effects are now in progress.

The authors wish to thank Professors Y. Koike amd T. Hasegawa for valuable discussions and are indebted to Professor C. F. Perdrisat for providing the details of his data.

References

[1] S. S. Vasan, Phys. Rev. D **8** (1973) 4092.

[2] A. P. Kobushkin et al., Phys. Rev. C **50** (1994) 2627.

[3] V. Punjabi et al., Phys. Lett. **B 350** (1995) 178.

[4] I. M. Sitnik, V. P. Ladygin and M. P. Rekalo, Phys. Atomic Nuclei **57** (1994) 2089; Yu. L. Dorodnykh and V. M. Kolybasov, Phys. Lett. **B333** (1994) 283; B. Kuehn, C. F. Perdrisat and E. A. Strokovsky, Phys. Atomic Nuclei **58** (1995) 1795; L. P. Kaptari et al., Phys. Lett. **B351** (1995) 400; A. P. Kobushkin and A. I. Syamtomov, Few-Body Syst. **8** (1995) 364.

[5] P. P. Rekalo and I. M. Sitnik, Phys. Lett. **B356** (1995) 434.

[6] M. Tanifuji and K. Yazaki, Prog. Theor. Phys. **40** (1968) 1023.

[7] M. Tanifuji, Phys. Lett. **B363** (1995) 151.

[8] M. Tanifuji, Phys. Lett. **B289** (1992) 233.

[9] M. Lacombe et al., Phys. Rev. C **21** (1980) 861.

[10] R. V. Reid, Ann. of Phys. **50** (1968) 411.

[11] M. M. Nagels, T. A. Rijken and J. J. de Swart, Phys. Rev. D **17** (1978) 768.

[12] R. Machleidt, Adv. Nucl. Phys. **19** (1989) 189.

[13] M. Yahiro et al., Prog. Theor. Phys. Suppl. **89** (1986) 32.

[14] A. Boudard and M. Dillig, Phys. Rev. C **31** (1985) 302.

[15] A. Nakamura and L. Satta, Nucl. Phys. **A 445** (1985) 706.

[16] J. Arvieux et al., Nucl. Phys. **A 431** (1984) 613.

Figure 1: Fourier transforms of deuteron internal wave functions. $u(k)$ and $w(k)$ are for the S and D components and k is the p-n relative momentum. The calculated are for the RSC (dash-dotted lines), Nijmegen (dotted lines), Paris (solid lines), and Bonn B (dashed lines) potentials. The zero point of $u(k)$, $k = k_0$, is shown by the arrow for the Paris potential for example.

Figure 2: T_{20} versus κ_0 $(=\frac{3}{2}K_y^y)$. The experimental data are for backward elastic scattering (open circles) and inclusive breakup (solid circles, only in (a)) [3]. The curves are calculated by Eqs. (10)-(12) and (15) for $\Theta = 180°$, $135°$, $120°$, $90°$ with $\Theta' = 0°$ in (a), for $\Theta' = 30°$, $60°$, $90°$ with Θ=135° in (b), for $\Theta' = -60°$, $-105°$, $-150°$ with $\Theta = 135°$ in (c) and for Θ'=60°, 105°, 120° with $\Theta = 180°$ in (d). The large circles are the PWIA calculation. In (d), the data points are connected by straight lines (see text).

Figure 3: T_{20}, κ_0 and K_{xz}^y versus k. The open circles are the experimental data for the backward elastic scattering [3]. The curves are calculated by Eqs. (10)-(12) and (15) with the Paris potential, where the lines are for (Θ, Θ')=(135°, 30°) [the solid], (135°, $-105°$) [the dashed], (180°, 105°) [the dotted] and (180°, 120°) [the dash-dotted]. The thin solid lines are the PWIA calculation, which gives zero for K_{xz}^y. The vertical dash-dotted straight line indicates the location of $k = k_0$.

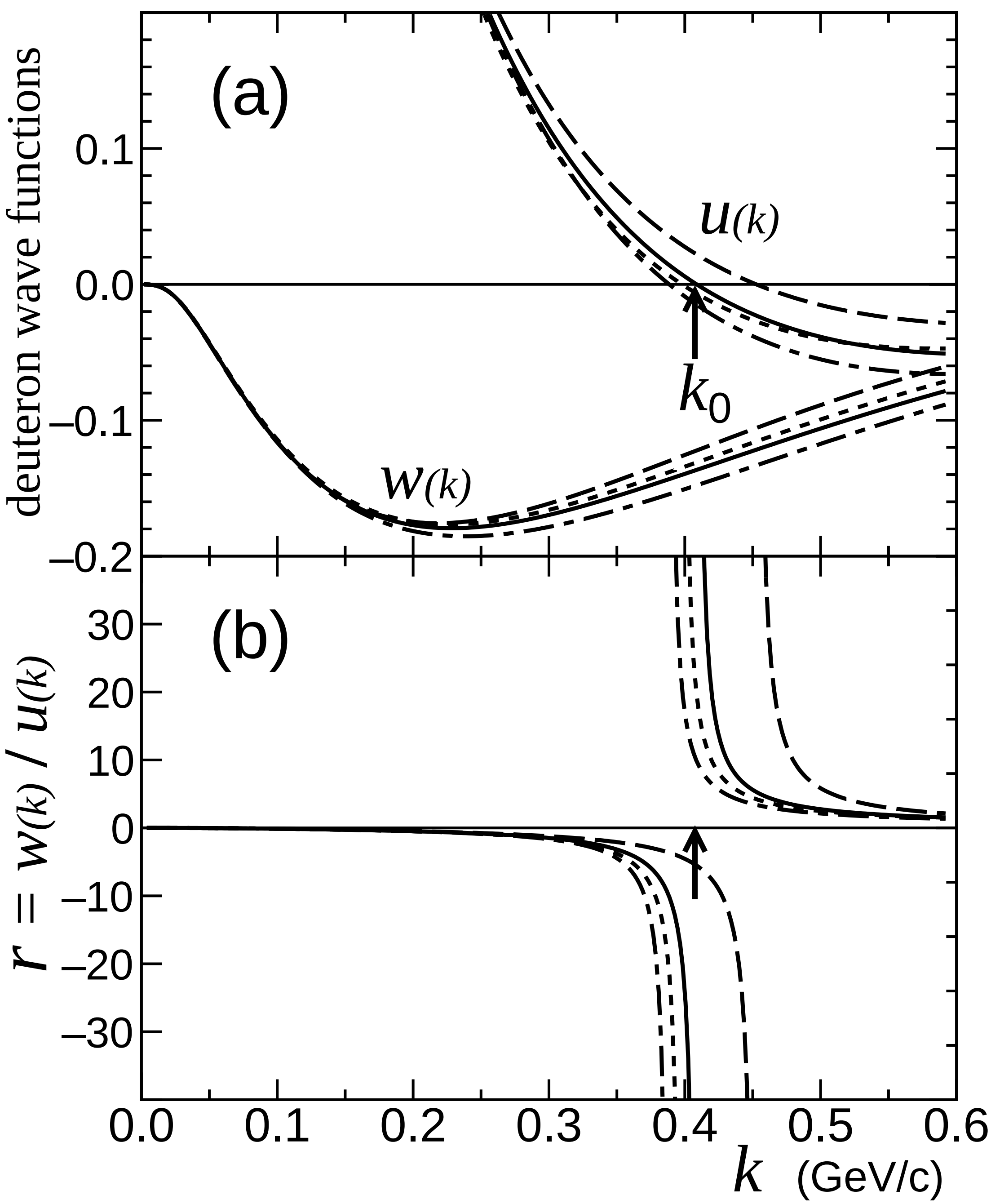

(a)
deuteron wave functions
0.1
0.0
−0.1
−0.2
u(k)
w(k)
k0
(b)
r = w(k) / u(k)
30
20
10
0
−10
−20
−30
0.0
0.1
0.2
0.3
0.4
0.5
0.6
k (GeV/c)

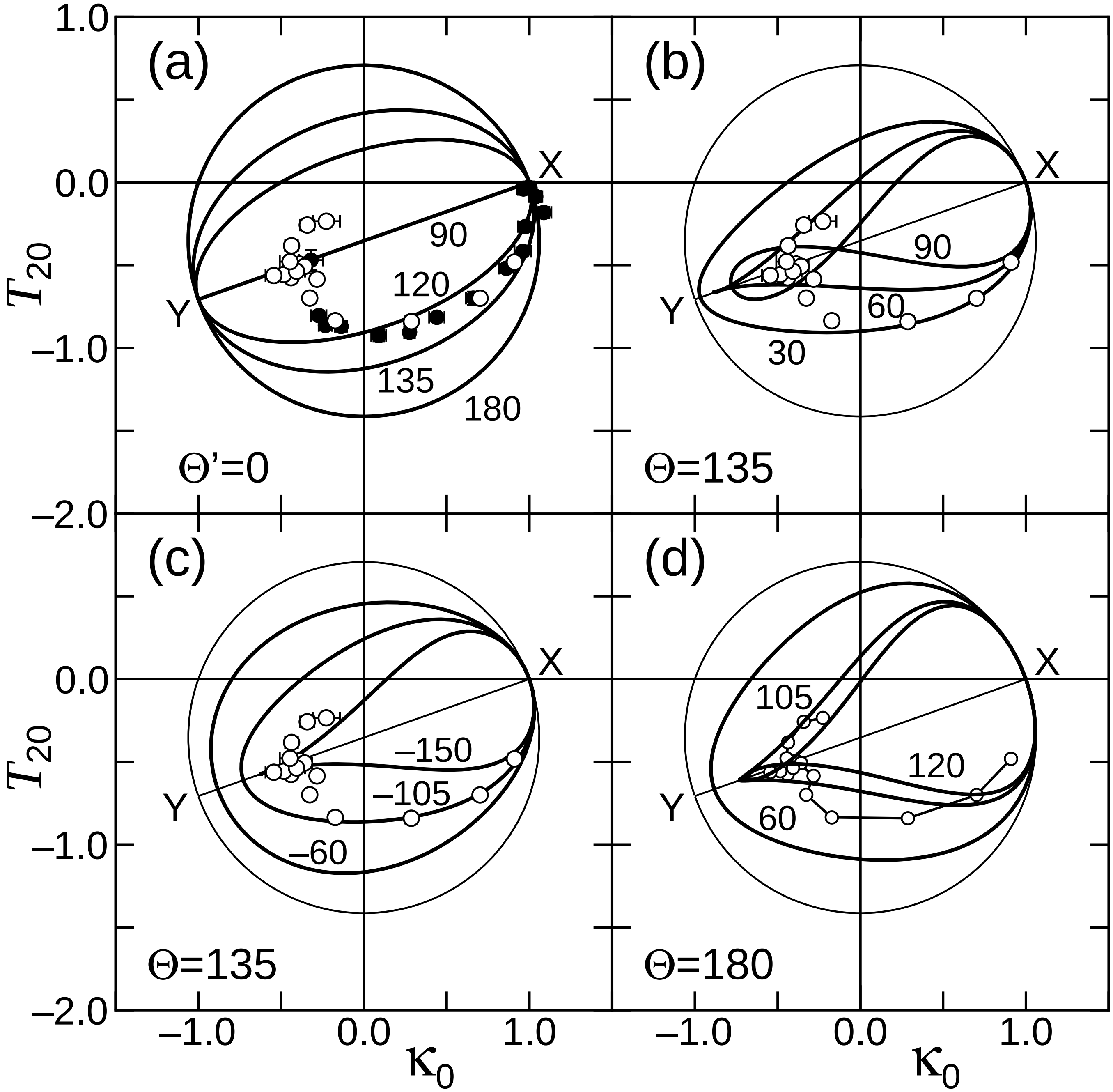

(a)
(b)
(c)
(d)
1.0
0.0
–1.0
–2.0
T_{20}
κ_0
–1.0
0.0
1.0
X
Y
90
120
135
180
Θ'=0
90
60
30
Θ=135
–150
–105
–60
Θ=135
105
120
60
Θ=180

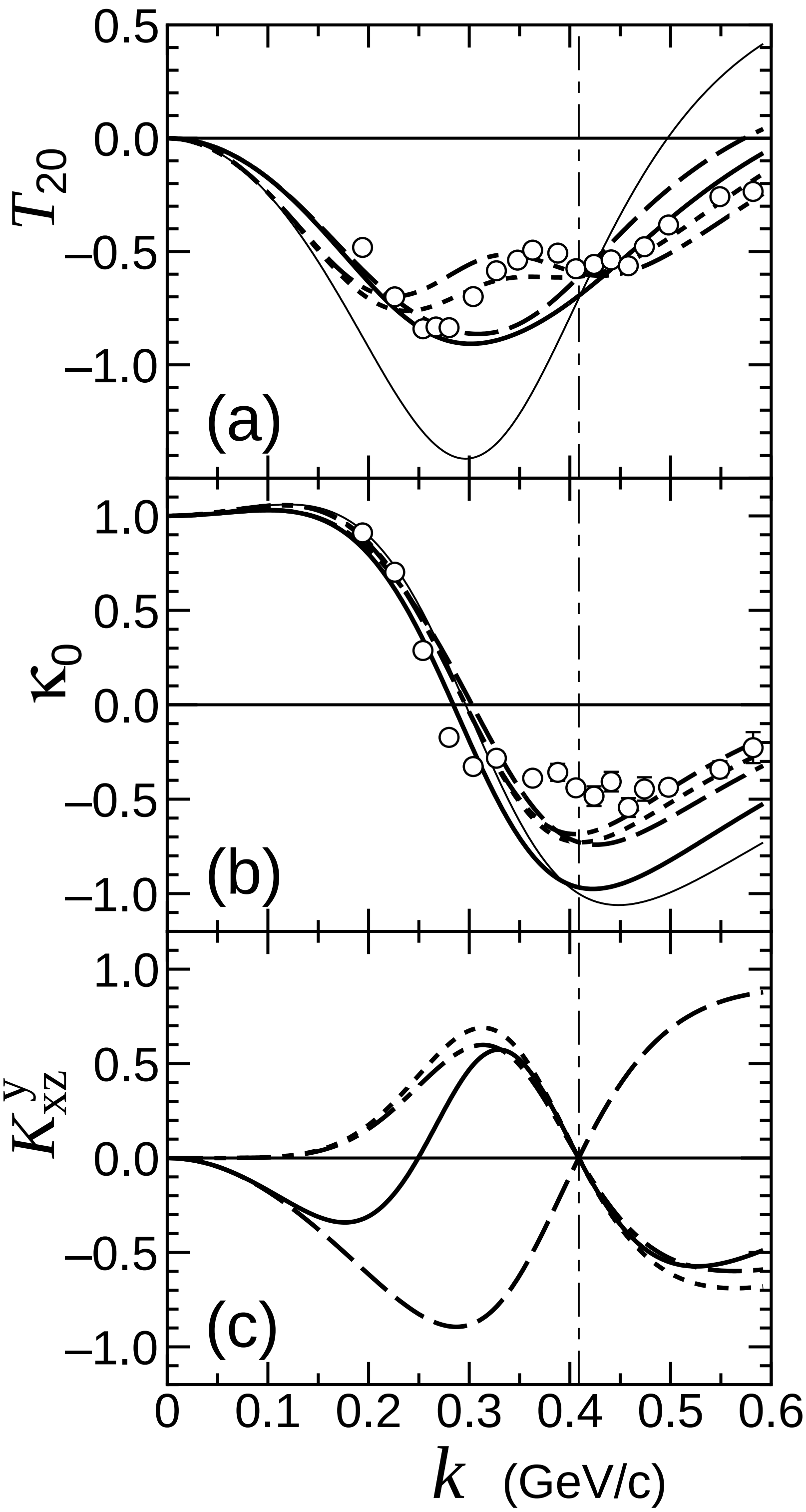

T_{20}
(a)
κ_0
(b)
K^y_{xz}
(c)
0.5
0.0
−0.5
−1.0
1.0
0 0.1 0.2 0.3 0.4 0.5 0.6
k (GeV/c)